

In-plane soil-structure interaction excited by incident plane SV waves

Yiwei Cai^a, Vincent W. Lee^b, Mihailo D. Trifunac^{b,*}

^a Department of Physics, University of Southern California, Los Angeles, CA 90089-0484, USA

^b Department of Civil Engineering, University of Southern California, Los Angeles, CA 90089-2531, USA



ARTICLE INFO

Keywords:

In-plane two dimensional soil-structure interaction
Incident SV waves
Relaxed half-space boundary conditions

ABSTRACT

In-plane soil-structure-interaction of a shear wall on a rigid circular foundation embedded in a linear elastic half-space, excited by an incident plane SV wave, is solved by relaxing the zero-stress boundary conditions on the ground surface. An approximate solution of this model was previously presented for the cylindrical approximation of the ground surface. This paper formally neglects such boundary conditions, and as a result, the complexity of the formulation is significantly reduced. Solutions for foundation and building motions in frequency space are compared to the previous results and it is shown that the present approximate solution provides excellent and almost identical results. The objective of this paper is to provide further insight on the role and the effects of surface boundary conditions for this type of problem.

1. Introduction

The study of soil-structure interaction (SSI) during seismic excitation by means of elementary models is an area that attracts continuing interest in earthquake engineering. In addition to solving such problems by numerical simulations such as finite elements, finite differences, and boundary integral methods, analytic approaches based on wave-function expansion have also shown to be successful in cases of simple foundation and building geometries. In addition to ease of computation, closed-form solutions help explore the underlying physics of the problem and serve as a reference to check the accuracy of numerical simulations. Among two-dimensional problems, cases of an incident plane SH wave was solved earliest by the method of images [1,2], which helps to satisfy the boundary condition on the ground surface through setting up wave functions that form the mirror symmetry with respect to this boundary. However, the image method does not work in cases of incident plane P or SV waves because of the coupled boundary conditions and the mode conversion between the two. As such, approximate analytic solutions based on the large circular approximation (LCA) – i.e. treating the ground surface as a surface of a large cylinder – has been the main early approach for analyzing in-plane motions. Examples of the LCA approach can be found in [3,4], and [5] in which the structure is modeled by a shear wall, or [6] in which the structure is represented by a single degree-of-freedom oscillator. More recently, studies based on relaxing (neglecting) the surface boundary conditions have been considered because of the expectation that results may be similar to those of the LCA [7]. Without resorting to the LCA, the methods of integral transform and conformal transform have been used

in models of surface and subsurface topographies and inclusions [8,9]. This paper presents a closer look at the model previously studied by [3] for the case of an incident plane SV wave. Solution procedures based on relaxing surface boundary conditions will be presented. It is expected that results on the comparison between “relaxed solutions” and LCA solutions will contribute to the library of solutions that address the problems discussed in [7]. For the present model with a rigid and circular foundation and for the flat half-space surface, it will be shown that relaxing the stress-free boundary conditions for the waves scattered from the foundation can lead to very good approximation, thereby suggesting that the effects caused by the presence of a half-space on cylindrical scattered waves should be small. For more irregular foundational geometries, and for nonlinear soil response in the foundation vicinity, such an approximation will cease to be useful [10–12].

2. Model and free-field

The model in Fig. 1 consists of a shear wall supported by a rigid circular foundation embedded in a semi-infinite half-space. The definition of parameters and coordinate systems used to describe the shear wall, foundation, and the half-space are as follows. The rectangular shear wall, referred to as the building, has width W , height H , and mass per unit length m_b . It consists of a uniform, linear, elastic medium with mass density ρ_b , Lamé constants (μ_b, λ_b) , Poisson ratio ν_b , longitudinal wave speed $c_{\alpha,b}$, and shear wave speed $c_{\beta,b}$. The foundation has a circular cross section, width $2a$, depth h , and a radius of curvature b at the circular portion, and the center of curvature is located at point O_1 . The distance between O_1 and the center of the building base O is d . The

* Corresponding author.

E-mail address: trifunac@usc.edu (M.D. Trifunac).

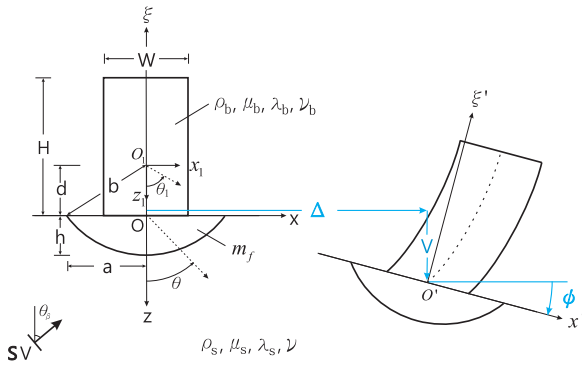


Fig. 1. The model.

depth h lies in the range of $0 < h \leq a$. The foundation material is assumed to be rigid and uniform, with mass per unit length m_f , and moment of inertia $I_o^{(f)}$ about point O . The half-space, representing the soil, is a uniform, linear, elastic medium with mass density ρ_s , Lamé constants (μ_s, λ_s) , Poisson ratio ν , longitudinal wave speed c_α , and shear wave speed c_β . Contact between the half-space and the foundation is assumed to be continuous with no relative slippage. An inertial coordinate system $O - x - z$ with origin O located at the center of the building base, and an inertial coordinate system $O_1 - x_1 - z_1$ with the origin located at O_1 , are used to describe the motion of the half-space. The polar variables in each of these coordinate systems are (r, θ) and (r_1, θ_1) , respectively. Also, an inertial coordinate system $O - x - \xi$, and a non-inertial coordinate system $O' - x' - \xi'$ that attaches to and moves with the building base are used to describe the motion of the building. The contact surface between the half-space and the foundation is denoted by $\Sigma: r_1 = b, -\theta_0 \leq \theta_1 \leq \theta_0$ with $\theta_0 = \sin^{-1}(a/b)$.

The steady state displacements of the foundation is

$$\Delta(t) = \Delta_0 e^{-i\omega t}, \tag{1a}$$

$$V(t) = V_0 e^{-i\omega t}, \tag{1b}$$

$$\phi(t) = \phi_0 e^{-i\omega t} \tag{1c}$$

with horizontal translation Δ_0 , vertical translation V_0 , and clockwise rotation about point O , ϕ_0 to be determined. The building moves as a shear wall where its horizontal and vertical displacements $u_b(\xi, t)$, $v_b(\xi, t)$ satisfy the wave equation with velocities $c_{\beta,b}$ and $c_{\alpha,b}$, respectively. With the condition that the base of the shear wall moves with the foundation, and the top of the shear wall is stress free, $u_b(\xi, t)$ and $v_b(\xi, t)$ can be solved. The generalized force (per unit length) with which the building is acting on the foundation to first order in foundation displacements is then

$$\begin{Bmatrix} f_z^{(bf)}(t) \\ f_x^{(bf)}(t) \\ \frac{M_o^{(bf)}(t)}{H} \end{Bmatrix} = m_b \omega^2 \left([K^{(b)}] + [C_g^{(b)}] \right) \begin{Bmatrix} V_0 \\ \Delta_0 \\ \phi_0 H \end{Bmatrix} e^{-i\omega t}, \tag{2}$$

where the superscript (bf) is used to denote the force components that the building is exerting onto the foundation, and M_o is the clockwise moment about point O . The matrices $[K^{(b)}]_{3 \times 3}$, $[C_g^{(b)}]_{3 \times 3}$ are both real. The relative response of the building is defined by

$$u_b^{rel}(\xi, t) = u_b(\xi, t) - (\Delta(t) + \phi(t)\xi), \tag{3}$$

$$v_b^{rel}(\xi, t) = v_b(\xi, t) + V(t). \tag{4}$$

The incident wave is a monochromatic plane SV wave whose propagation vector lies in the $x - z$ plane with incident angle θ_β , harmonic frequency ω , wave number $k_\beta = \omega/c_\beta$, and incident amplitude ψ_0 . The presence of the half-space surface results in reflected SV and P waves. Together with the incident wave, the potentials are

$$\text{Incident SV-wave: } \psi^{(i)}(x, z, t) = \psi_0 e^{ik_\beta(x \sin \theta_\beta - z \cos \theta_\beta) - i\omega t}, \tag{5a}$$

$$\text{Reflected SV-wave: } \psi^{(r)}(x, z, t) = \psi_0 K_2 e^{ik_\beta(x \sin \theta_\beta + z \cos \theta_\beta) - i\omega t}, \tag{5b}$$

$$\text{Reflected P-wave: } \varphi^{(r)}(x, z, t) = \psi_0 K_1 e^{ik_\alpha(x \sin \theta_\alpha + z \cos \theta_\alpha) - i\omega t}, \tag{5c}$$

where $k_\alpha = \omega/c_\alpha$ is the wave number of the reflected P wave, θ_α is the angle of the reflected P wave and satisfies

$$\sin \theta_\alpha = \kappa \sin \theta_\beta, \tag{6}$$

where $\kappa = \frac{c_\alpha}{c_\beta} = \frac{k_\beta}{k_\alpha}$ is the ratio of speeds of the longitudinal to the shear wave. The ratios of the reflected to incident amplitudes are

$$K_1 = \frac{2\kappa^2 \sin 2\theta_\beta \cos 2\theta_\beta}{\sin 2\theta_\alpha \sin 2\theta_\beta + \kappa^2 \cos^2 2\theta_\beta},$$

$$K_2 = \frac{\sin 2\theta_\alpha \sin 2\theta_\beta - \kappa^2 \cos^2 2\theta_\beta}{\sin 2\theta_\alpha \sin 2\theta_\beta + \kappa^2 \cos^2 2\theta_\beta}. \tag{7}$$

The free-field potentials now consist of

$$\varphi^{ff} = \varphi^{(r)},$$

$$\psi^{ff} = \psi^{(i)} + \psi^{(r)}. \tag{8}$$

The harmonic time dependence $e^{-i\omega t}$ will be associated with all steady-state wave potentials and omitted in subsequent equations.

3. Solution of the problem

The presence of the foundation induces scattered waves. The representations of scattered P and SV potentials are given by the Fourier-Hankel series:

$$\varphi^s(r_1, \theta_1) = \sum_{n=0}^N H_n^{(1)}(k_\alpha r_1) [A_n \sin n\theta_1 + B_n \cos n\theta_1],$$

$$\psi^s(r_1, \theta_1) = \sum_{n=0}^N H_n^{(1)}(k_\beta r_1) [C_n \sin n\theta_1 + D_n \cos n\theta_1] \tag{9}$$

for some numerical order N . The 4 sets of scattered wave coefficients $\{A_n\}_{n=0}^N$, $\{B_n\}_{n=0}^N$, $\{C_n\}_{n=0}^N$, and $\{D_n\}_{n=0}^N$ are to be determined by boundary conditions between the half-space and the foundation.

Unlike the case of an incident P wave, the reflected P wave $\varphi^{(r)}$ for an SV incident wave here can be either a body wave or a surface wave depending on the incident angle. The critical angle

$$\sin \theta_{cr} = \frac{1}{\kappa} \tag{10}$$

separates these two cases. If the incidence is below critical angle ($\theta_\beta < \theta_{cr}$), θ_α is real-valued and $\varphi^{(r)}$ is a plane-traveling wave. In this case, the Fourier-Bessel expansion of the free-fields can be represented as follows:

$$\varphi^{ff}(r_1, \theta_1) = \sum_{n=0}^{\infty} J_n(k_\alpha r_1) [a_n \sin n\theta_1 + b_n \cos n\theta_1], \tag{11a}$$

$$\psi^{ff}(r_1, \theta_1) = \sum_{n=0}^{\infty} J_n(k_\beta r_1) [c_n \sin n\theta_1 + d_n \cos n\theta_1], \tag{11b}$$

with the free-field coefficients

$$a_n = \psi_0 \varepsilon_n i^n K_1 e^{-ik_\alpha d \cos \theta_\alpha} \sin n\theta_\alpha, \tag{12a}$$

$$b_n = \psi_0 \varepsilon_n i^n K_1 e^{-ik_\alpha d \cos \theta_\alpha} \cos n\theta_\alpha, \tag{12b}$$

$$c_n = \psi_0 \varepsilon_n i^n \sin n\theta_\beta [-(-1)^n e^{ik_\beta d \cos \theta_\beta} + K_2 e^{-ik_\beta d \cos \theta_\beta}], \tag{12c}$$

$$d_n = \psi_0 \varepsilon_n i^n \cos n\theta_\beta [(-1)^n e^{ik_\beta d \cos \theta_\beta} + K_2 e^{-ik_\beta d \cos \theta_\beta}]. \tag{12d}$$

If the incidence is beyond critical angle ($\theta_\beta > \theta_{cr}$), θ_α is complex-valued. Let

$$k_x = k_\beta \sin \theta_\beta \tag{13}$$

be the apparent wave number, then $\sin \theta_\alpha = k_x/k_\alpha$. Using the fact that $\varphi^{(r)}$ satisfies the Helmholtz equation: $\nabla^2 \varphi^{(r)} + k_\alpha^2 \varphi^{(r)} = 0$, it can be deduced that $\cos \theta_\alpha = i\gamma/k_\alpha$ with the following definition:

$$\gamma \equiv \sqrt{k_x^2 - k_\alpha^2} > 0. \tag{14}$$

In terms of the two real numbers k_x and γ , $\varphi^{(r)}$ can then be rewritten as $\varphi^{(r)}(x, z) = \psi_0 K_1 e^{ik_x x - \gamma z}$,

$$\tag{15}$$

and (15) represents a surface wave with exponentially decaying amplitude into the half-space $z > 0$.

The solution procedures for incidence beyond critical angle will be different when the incidence is below critical. Since the Fourier-Bessel series of $\varphi^{(r)}$ in (11a), (12a), and (12b) are no longer valid in such a case, (15) will be used directly to derive the P-wave portion of the displacements and stresses at the contact surface Σ before the series expansions are made. In terms of coordinate system (r_1, θ_1) , (15) is equal to

$$\varphi^r(r_1, \theta_1) = \psi_0 K_1 e^{\gamma d} e^{f(\theta_1) r_1} \tag{16}$$

with a complex function of θ_1

$$f(\theta_1) = ik_x \sin \theta_1 - \gamma \cos \theta_1. \tag{17}$$

Each of the displacement and stress components can be grouped according to the contribution from either the P or SV potential:

$$\begin{aligned} u_{r_1} &= u_{r_1}^{(P)} + u_{r_1}^{(SV)}, \\ u_{\theta_1} &= u_{\theta_1}^{(P)} + u_{\theta_1}^{(SV)}, \end{aligned} \tag{18}$$

$$\begin{aligned} \tau_{r_1 r_1} &= \tau_{r_1 r_1}^{(P)} + \tau_{r_1 r_1}^{(SV)}, \\ \tau_{r_1 \theta_1} &= \tau_{r_1 \theta_1}^{(P)} + \tau_{r_1 \theta_1}^{(SV)}, \end{aligned} \tag{19}$$

$$\begin{aligned} u_{r_1}^{(P)}(r_1, \theta_1) &= \frac{\partial \varphi}{\partial r_1}, \\ u_{\theta_1}^{(P)}(r_1, \theta_1) &= \frac{1}{r_1} \frac{\partial \varphi}{\partial \theta_1}, \end{aligned} \tag{20}$$

$$\begin{aligned} \tau_{r_1 r_1}^{(P)}(r_1, \theta_1) &= -\lambda_s k_\alpha^2 \varphi + 2\mu_s \frac{\partial^2 \varphi}{\partial r_1^2}, \\ \tau_{r_1 \theta_1}^{(P)}(r_1, \theta_1) &= \frac{2\mu_s}{r_1^2} \left[r_1 \frac{\partial^2 \varphi}{\partial r_1 \partial \theta_1} - \frac{\partial \varphi}{\partial \theta_1} \right]. \end{aligned} \tag{21}$$

Substituting (16) as φ into (20) and (21) and evaluating at Σ yields

$$u_{r_1}^{(P)}(b, \theta_1) = \psi_0 K_1 e^{\gamma d} f(\theta_1) e^{f(\theta_1) b}, \tag{22a}$$

$$u_{\theta_1}^{(P)}(b, \theta_1) = \psi_0 K_1 e^{\gamma d} \frac{df(\theta_1)}{d\theta_1} e^{f(\theta_1) b}, \tag{22b}$$

$$\tau_{r_1 r_1}^{(P)}(b, \theta_1) = [-\lambda_s k_\alpha^2 + 2\mu_s f^2(\theta_1)] \psi_0 K_1 e^{\gamma d} e^{f(\theta_1) b}, \tag{23a}$$

$$\tau_{r_1 \theta_1}^{(P)}(b, \theta_1) = 2\mu_s f(\theta_1) \frac{df(\theta_1)}{d\theta_1} \psi_0 K_1 e^{\gamma d} e^{f(\theta_1) b} \tag{23b}$$

for all $-\theta_0 \leq \theta_1 \leq \theta_0$. To apply the boundary conditions, it is necessary to obtain the Fourier θ_1 -expansion of each function in (22) and (23), which requires the definition of these functions above the physical domain of Σ . Due to the exponentially growing magnitude of $\varphi^{(r)}$ above the half-space, direct extensions of the existing definitions of (22) and (23) to above the physical domain are not appropriate, nor are simple truncations that incur Gibbs phenomena. Let the extensions be $z_{i,ext}(\theta_1)$, $i = 1, \dots, 4$ so that the full-range definitions are

$$\bar{u}_{r_1}^{(P)}(b, \theta_1) = \begin{cases} u_{r_1}^{(P)}(b, \theta_1) = \psi_0 K_1 e^{\gamma d} f(\theta_1) e^{f(\theta_1) b}, & -\theta_0 \leq \theta_1 \leq \theta_0, \\ z_{1,ext}(\theta_1), & \theta_0 \leq \theta_1 \leq (2\pi - \theta_0), \end{cases} \tag{24}$$

$$\bar{u}_{\theta_1}^{(P)}(b, \theta_1) = \begin{cases} u_{\theta_1}^{(P)}(b, \theta_1) = \psi_0 K_1 e^{\gamma d} \frac{df(\theta_1)}{d\theta_1} e^{f(\theta_1) b}, & -\theta_0 \leq \theta_1 \leq \theta_0, \\ z_{2,ext}(\theta_1), & \theta_0 \leq \theta_1 \leq (2\pi - \theta_0), \end{cases} \tag{25}$$

$$\bar{\tau}_{r_1 r_1}^{(P)}(b, \theta_1) = \begin{cases} \tau_{r_1 r_1}^{(P)}(b, \theta_1) = [-\lambda k_\alpha^2 & -\theta_0 \leq \theta_1 \leq \theta_0, \\ + 2\mu f^2(\theta_1)] \psi_0 K_1 e^{\gamma d} e^{f(\theta_1) b}, & \\ z_{3,ext}(\theta_1), & \theta_0 \leq \theta_1 \leq (2\pi - \theta_0), \end{cases} \tag{26}$$

$$\bar{\tau}_{r_1 \theta_1}^{(P)}(b, \theta_1) = \begin{cases} \tau_{r_1 \theta_1}^{(P)}(b, \theta_1) = 2\mu f(\theta_1) \frac{df(\theta_1)}{d\theta_1} \psi_0 K_1 e^{\gamma d} e^{f(\theta_1) b}, & -\theta_0 \leq \theta_1 \leq \theta_0, \\ z_{4,ext}(\theta_1), & \theta_0 \leq \theta_1 \leq (2\pi - \theta_0). \end{cases} \tag{27}$$

The $z_{i,ext}(\theta_1)$'s are thus constructed so that they make $\bar{u}_{r_1}^{(P)}$, $\bar{u}_{\theta_1}^{(P)}$, $\bar{\tau}_{r_1 r_1}^{(P)}$, and $\bar{\tau}_{r_1 \theta_1}^{(P)}$ continuous periodic functions of θ_1 with comparable magnitudes everywhere in $-\pi \leq \theta_1 \leq \pi$, and also to produce the proper asymptotic behavior at the zero frequency limit. More specifically, $z_{i,ext}$'s are taken to be functions of θ_1 and η of the form

$$z_{i,ext}(\theta_1, \eta) = w(\eta) z_i(\theta_1, \eta) + (1 - w(\eta)) L_i(\theta_1, \eta), \quad i = 1, \dots, 4, \tag{28}$$

where $z_i(\theta_1, \eta)$'s are the same functions as those defined within $|\theta_1| \leq \theta_0$ in (24) through (27), $L_i(\theta_1, \eta)$'s are 4 linear functions of θ_1 joining the two edge values $z_{i,r} = z_i(\theta_0, \eta)$, $z_{i,l} = z_i(-\theta_0, \eta)$ of $z_i(\theta_1, \eta)$:

$$L_i(\theta_1, \eta) = \begin{cases} z_{i,r} + \frac{z_{i,l} - z_{i,r}}{2(\pi - \theta_0)} (\theta_1 - \theta_0), & \theta_0 \leq \theta_1 \leq \pi, \\ z_{i,l} + \frac{z_{i,l} - z_{i,r}}{2(\pi - \theta_0)} (\theta_1 + \theta_0), & -\pi \leq \theta_1 \leq -\theta_0, \end{cases} \tag{29}$$

and $w(\eta)$ is a linear transition function of η :

$$w(\eta) = \begin{cases} -2\eta + 1, & \eta \leq 0.5, \\ 0, & \eta > 0.5 \end{cases} \tag{30}$$

making each $z_{i,ext}(\theta_1, \eta)$ gradually evolve from $z_i(\theta_1, \eta)$ at $\eta = 0$ to $L_i(\theta_1, \eta)$ at $\eta = 0.5$ and beyond. In other words, each extension evolve from the corresponding direct extension to a linear extension as frequency increases between 0 and 0.5. Since the transition function is also continuous, the resulting full-range definition is continuous in θ_1 at all frequencies.

The finite Fourier series of (24) through (27) are

$$\bar{u}_{r_1}^{(P)}(b, \theta_1) = \frac{1}{b} \sum_{n=0}^{N_f-1} [a_n^{(ur)} \sin n\theta_1 + b_n^{(ur)} \cos n\theta_1], \tag{31a}$$

$$\bar{u}_{\theta_1}^{(P)}(b, \theta_1) = \frac{1}{b} \sum_{n=0}^{N_f-1} [a_n^{(ut)} \sin n\theta_1 + b_n^{(ut)} \cos n\theta_1], \tag{31b}$$

$$\bar{\tau}_{r_1 r_1}^{(P)}(b, \theta_1) = \frac{2\mu_s}{b^2} \sum_{n=0}^{N_f-1} [a_n^{(sr)} \sin n\theta_1 + b_n^{(sr)} \cos n\theta_1], \tag{32a}$$

$$\bar{\tau}_{r_1 \theta_1}^{(P)}(b, \theta_1) = \frac{2\mu_s}{b^2} \sum_{n=0}^{N_f-1} [a_n^{(st)} \sin n\theta_1 + b_n^{(st)} \cos n\theta_1], \tag{32b}$$

where the 8 sets of coefficients $\{a_n^{(ur)}\}_{n=0}^{N_f-1}$, $\{b_n^{(ur)}\}_{n=0}^{N_f-1}$, $\{a_n^{(ut)}\}_{n=0}^{N_f-1}$, $\{b_n^{(ut)}\}_{n=0}^{N_f-1}$, $\{a_n^{(sr)}\}_{n=0}^{N_f-1}$, $\{b_n^{(sr)}\}_{n=0}^{N_f-1}$, $\{a_n^{(st)}\}_{n=0}^{N_f-1}$, and $\{b_n^{(st)}\}_{n=0}^{N_f-1}$ are determined by

$$\begin{aligned}
 a_0^{(ur)} &= 0, \\
 b_0^{(ur)} &= \frac{1}{2N_f} \sum_{l=0}^{2N_f-1} b \bar{u}_{r_1}^{(P)}(b, \theta_l), \\
 a_n^{(ur)} &= \frac{1}{N_f} \sum_{l=0}^{2N_f-1} b \bar{u}_{r_1}^{(P)}(b, \theta_l) \sin n\theta_l, \quad n = 1, 2, \dots, N_f - 1, \\
 b_n^{(ur)} &= \frac{1}{N_f} \sum_{l=0}^{2N_f-1} b \bar{u}_{r_1}^{(P)}(b, \theta_l) \cos n\theta_l, \quad n = 1, 2, \dots, N_f - 1,
 \end{aligned} \tag{33}$$

$$\begin{aligned}
 a_0^{(ut)} &= 0, \\
 b_0^{(ut)} &= \frac{1}{2N_f} \sum_{l=0}^{2N_f-1} b \bar{u}_{\theta_1}^{(P)}(b, \theta_l), \\
 a_n^{(ut)} &= \frac{1}{N_f} \sum_{l=0}^{2N_f-1} b \bar{u}_{\theta_1}^{(P)}(b, \theta_l) \sin n\theta_l, \quad n = 1, 2, \dots, N_f - 1, \\
 b_n^{(ut)} &= \frac{1}{N_f} \sum_{l=0}^{2N_f-1} b \bar{u}_{\theta_1}^{(P)}(b, \theta_l) \cos n\theta_l, \quad n = 1, 2, \dots, N_f - 1,
 \end{aligned} \tag{34}$$

$$\begin{aligned}
 a_0^{(sr)} &= 0, \\
 b_0^{(sr)} &= \frac{1}{2N_f} \sum_{l=0}^{2N_f-1} \frac{b^2}{2\mu_s} \bar{\tau}_{r_1 r_1}^{(P)}(b, \theta_l), \\
 a_n^{(sr)} &= \frac{1}{N_f} \sum_{l=0}^{2N_f-1} \frac{b^2}{2\mu_s} \bar{\tau}_{r_1 r_1}^{(P)}(b, \theta_l) \sin n\theta_l, \quad n = 1, 2, \dots, N_f - 1, \\
 b_n^{(sr)} &= \frac{1}{N_f} \sum_{l=0}^{2N_f-1} \frac{b^2}{2\mu_s} \bar{\tau}_{r_1 r_1}^{(P)}(b, \theta_l) \cos n\theta_l, \quad n = 1, 2, \dots, N_f - 1,
 \end{aligned} \tag{35}$$

$$\begin{aligned}
 a_0^{(st)} &= 0, \\
 b_0^{(st)} &= \frac{1}{2N_f} \sum_{l=0}^{2N_f-1} \frac{b^2}{2\mu_s} \bar{\tau}_{r_1 \theta_1}^{(P)}(b, \theta_l), \\
 a_n^{(st)} &= \frac{1}{N_f} \sum_{l=0}^{2N_f-1} \frac{b^2}{2\mu_s} \bar{\tau}_{r_1 \theta_1}^{(P)}(b, \theta_l) \sin n\theta_l, \quad n = 1, 2, \dots, N_f - 1, \\
 b_n^{(st)} &= \frac{1}{N_f} \sum_{l=0}^{2N_f-1} \frac{b^2}{2\mu_s} \bar{\tau}_{r_1 \theta_1}^{(P)}(b, \theta_l) \cos n\theta_l, \quad n = 1, 2, \dots, N_f - 1.
 \end{aligned} \tag{36}$$

The summations in (33), (34), (35), (36) are over the space of the $2N_f$ -discretized θ_l :

$$\theta_l = \frac{\pi}{N_f} l, \quad l = 0, 1, 2, \dots, (2N_f - 1). \tag{37}$$

The displacements at the contact surface resulting from the total potentials

$$\begin{aligned}
 \varphi &= \varphi^{ff} + \varphi^s, \\
 \psi &= \psi^{ff} + \psi^s
 \end{aligned} \tag{38}$$

become

$$\begin{aligned}
 \left\{ \begin{matrix} u_{r_1} \\ u_{\theta_1} \end{matrix} \right\}_{\Sigma} &= \frac{1}{b} \sum_{n=0}^{\infty} [S_n(\theta_1)] \left\{ \begin{matrix} a_n^{(ur)} - D_{12}^{(1)}(n, b)d_n \\ b_n^{(ut)} + D_{22}^{(1)}(n, b)d_n \end{matrix} \right\} + [D^{(3)-}(n, b)] \left\{ \begin{matrix} A_n \\ D_n \end{matrix} \right\} \\
 &+ \frac{1}{b} \sum_{n=0}^{\infty} [C_n(\theta_1)] \left\{ \begin{matrix} b_n^{(sr)} + D_{12}^{(1)}(n, b)c_n \\ a_n^{(st)} + D_{22}^{(1)}(n, b)c_n \end{matrix} \right\} + [D^{(3)+}(n, b)] \left\{ \begin{matrix} B_n \\ C_n \end{matrix} \right\}.
 \end{aligned} \tag{39}$$

Similarly, the total stresses at the contact surface become

$$\begin{aligned}
 \left\{ \begin{matrix} \tau_{r_1 r_1} \\ \tau_{r_1 \theta_1} \end{matrix} \right\}_{\Sigma} &= \frac{2\mu_s}{b^2} \sum_{n=0}^{\infty} [S_n(\theta_1)] \left\{ \begin{matrix} a_n^{(sr)} - E_{12}^{(1)}(n, b)d_n \\ b_n^{(st)} + E_{42}^{(1)}(n, b)d_n \end{matrix} \right\} \\
 &+ [E^{(3)-}(n, b)] \left\{ \begin{matrix} A_n \\ D_n \end{matrix} \right\} \\
 &+ \frac{2\mu_s}{b^2} \sum_{n=0}^{\infty} [C_n(\theta_1)] \left\{ \begin{matrix} b_n^{(sr)} + E_{12}^{(1)}(n, b)c_n \\ a_n^{(st)} + E_{42}^{(1)}(n, b)c_n \end{matrix} \right\} \\
 &+ [E^{(3)+}(n, b)] \left\{ \begin{matrix} B_n \\ C_n \end{matrix} \right\}.
 \end{aligned} \tag{40}$$

The remaining derivations are the same as in the case of an incident P wave: the scattered coefficients are first eliminated through the displacement boundary conditions on Σ when deriving equations of the generalized forces with which the half-space is acting on the foundation. Thereafter, through the requirement that the foundation itself satisfies the dynamic equilibrium, the foundation displacements can be solved. Consequently, the end equation is

$$\left\{ \begin{matrix} V_0 \\ \Delta_0 \\ \phi_0 H \end{matrix} \right\} = \left(-\omega^2 [M^{(f)}] - m_b \omega^2 ([K^{(b)}]) + [C_g^{(b)}] - \frac{2\mu_s}{b} \sum_{n=0}^N [X_6(n)] \right)^{-1} \frac{2\mu_s}{b} \sum_{n=0}^N \{X_5(n)\}, \tag{41}$$

with the modified definitions

$$\{X_5(n)\}_{3 \times 1} = \left\{ \begin{matrix} [I_1(n) \quad -I_4(n)]_{1 \times 2} \{X_3(n)\}_{2 \times 1} \\ I_4(n) \quad I_1(n) \\ \left[\frac{d}{H} I_4(n) \quad -\frac{b}{H} I_5(n) + \frac{d}{H} I_1(n) \right]_{2 \times 2} \{X_1(n)\}_{2 \times 1} \end{matrix} \right\}, \tag{42}$$

where

$$\begin{aligned}
 \{X_1(n)\}_{2 \times 1} &= \left\{ \begin{matrix} a_n^{(sr)} - E_{12}^{(1)}(n, b)d_n \\ b_n^{(st)} + E_{42}^{(1)}(n, b)d_n \end{matrix} \right\} \\
 &- [E^{(3)-}(n, b)] [D^{(3)-}(n, b)]^{-1} \left\{ \begin{matrix} a_n^{(ur)} - D_{12}^{(1)}(n, b)d_n \\ b_n^{(ut)} + D_{22}^{(1)}(n, b)d_n \end{matrix} \right\},
 \end{aligned} \tag{43}$$

$$\begin{aligned}
 \{X_3(n)\}_{2 \times 1} &= \left\{ \begin{matrix} b_n^{(sr)} + E_{12}^{(1)}(n, b)c_n \\ a_n^{(st)} + E_{42}^{(1)}(n, b)c_n \end{matrix} \right\} \\
 &- [E^{(3)+}(n, b)] [D^{(3)+}(n, b)]^{-1} \left\{ \begin{matrix} b_n^{(sr)} + D_{12}^{(1)}(n, b)c_n \\ a_n^{(st)} + D_{22}^{(1)}(n, b)c_n \end{matrix} \right\}.
 \end{aligned} \tag{44}$$

4. Numerical results

A dimensionless frequency $\eta = \frac{2a}{\lambda_\beta} = \frac{\omega a}{\pi c_\beta}$, and the flexibility parameter of the building $\varepsilon = \frac{c_\beta H}{c_\beta b a}$ will be used in the figures showing the results. For all computations, the fixed parameters are $m_f/m_s = 0.2$, $\frac{g}{(c_\beta b \pi / 2 H)^2 a} = 10^{-4}$, and ν is slightly adjusted to the value $\nu = 0.3333 \approx 1/3$, which gives the critical angle of $\theta_{cr} = 30.0025^\circ \approx 30^\circ$. The amplitude of the incident SV wave is taken to be $\psi_0 = a/k_\beta$. These choices are adopted to facilitate comparison of the results with those in [3].

In Figs. 2–9, the amplitude spectra of the foundation displacements (Δ_0, ϕ_0, V_0) and the relative responses of the building ($u_b^{rel}(H), v_b^{rel}(H)$) are plotted in the range $0 < \eta \leq 2$ for 4 different geometries of the model, with angles of incidence $\theta_\beta = 0^\circ, 30^\circ, 45^\circ, 60^\circ$, and 85° of the incoming SV wave. Figs. 2–5 show the case of a shallow foundation, while Figs. 6–9 a semi-circular foundation. Figs. 2, 3, 6 and 7 are shown for a “square” shear wall. Figs. 4, 5, 8 and 9 correspond to a tall shear

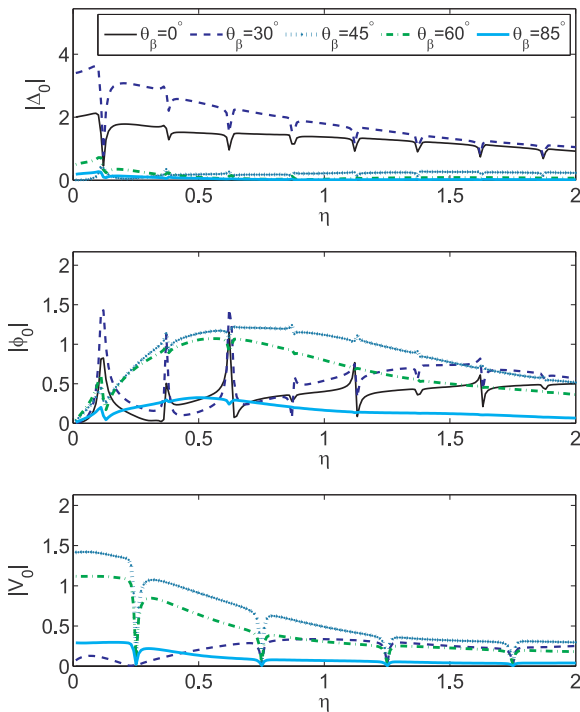


Fig. 2. Spectra of foundation displacements from "relaxed" solutions. $a/h = 2$, $W/H = 1$, $H/a = 2$, $m_b/m_f = 4$, and $\varepsilon = 4$.

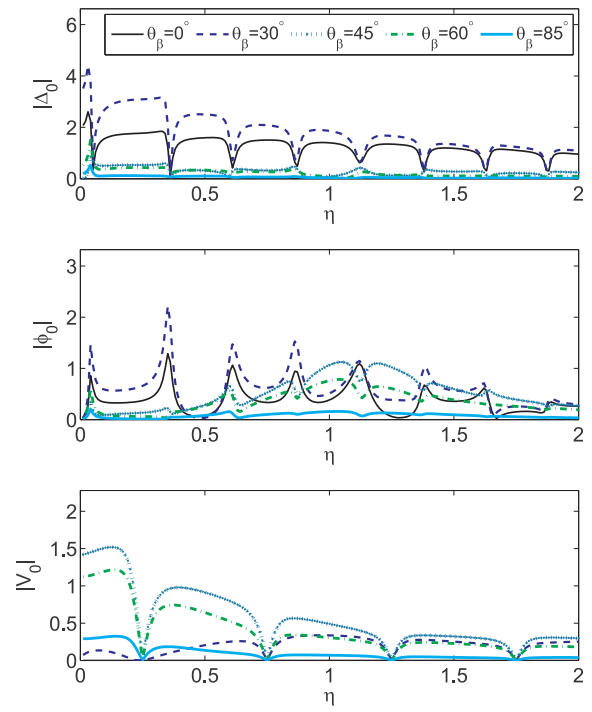


Fig. 4. Spectra of foundation displacements from "relaxed" solutions. $a/h = 2$, $W/H = 0.25$, $H/a = 8$, $m_b/m_f = 16$, and $\varepsilon = 4$.

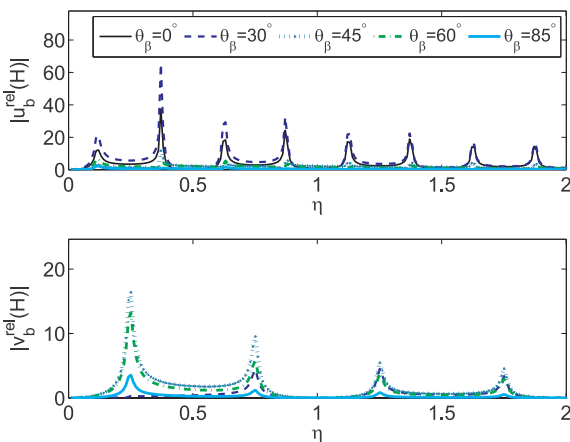


Fig. 3. Spectra of relative displacements of the shear wall from "relaxed" solutions. $a/h = 2$, $W/H = 1$, $H/a = 2$, $m_b/m_f = 4$, and $\varepsilon = 4$.

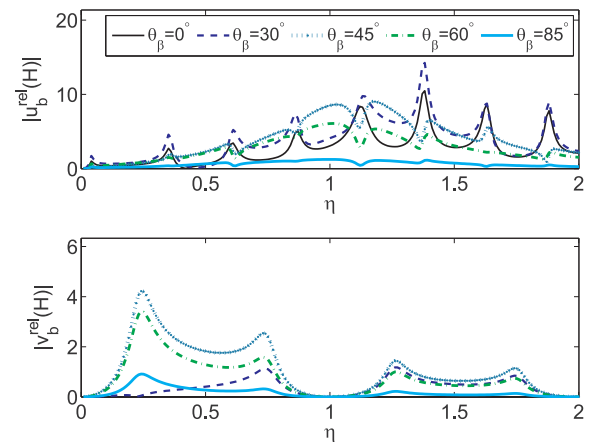


Fig. 5. Spectra of relative displacements of the shear wall from "relaxed" solutions. $a/h = 2$, $W/H = 0.25$, $H/a = 8$, $m_b/m_f = 16$, and $\varepsilon = 4$.

wall. It can be seen that the response spectra corresponding to a semi-circular foundation, as well as a shallow foundation with below critical incidence ($\theta_\beta < \theta_{cr}$) are all in good agreement with the results presented in [3]. Results for a shallow foundation for wave incidence beyond critical angle ($\theta_\beta > \theta_{cr}$) are not presented in [3] because of the lack of convergence described by the authors. The convergent issues do not exist here because of the less complicated mathematical form of the closed-form solution, thus the corresponding results are also shown in Figs. 2–5.

When frequency η approaches zero, the half-space motion is uniform, thus the translational amplitudes of the foundation approach the displacement amplitudes of the free-field on the ground surface, and the rotation of the foundation approaches zero. As η increases across each of the fixed-base natural frequencies of the building's horizontal/vertical oscillation, due to the singularity of the shear wall matrix $[K^{(b)}]$, the horizontal/vertical response spectra of the foundation and building experience rapid changes with local maxima or minima. Since rotation is coupled to horizontal motion, $|\phi_0|$ experiences resonant behavior at

horizontal fixed-base natural frequencies.

Away from the fixed-base natural frequencies, it can be seen that because of the filtering effect of the rigid foundation, the translational response $|\Delta_0|$ and $|V_0|$ decrease gradually from their zero-frequency limit as η increases from zero for most incident angles. The opposite trends are for $|\Delta_0|$ at $\theta_\beta = 45^\circ$ and for $|V_0|$ at $\theta_\beta = 30^\circ$. These two cases both correspond to a nearly zero response at zero-frequency limit ($|\Delta_0| \rightarrow 0$ at $\theta_\beta = 45^\circ$ and $|V_0| \rightarrow 0.0415$ at $\theta_\beta = 30^\circ$), because the horizontal free-field displacement amplitude on the ground surface ($|u_z^{ff}(z=0)|$) is zero at $\theta_\beta = 45^\circ$, and the vertical free-field displacement amplitude on the ground surface ($|v_z^{ff}(z=0)|$) is small with $|u_z^{ff}(z=0)| = 0.0415$ at $\theta_\beta = 30^\circ$. The gradual increases of $|\Delta_0|$ and $|V_0|$ beyond zero frequency show that the interaction between the incident wave and the foundation can create additional motions. Nevertheless, at higher frequencies, especially when η is approaching 2, the filtering effect of the foundation becomes dominant, and thus $|\Delta_0|$ and $|V_0|$ either saturate or begin to decrease.

For rotation spectra $|\phi_0|$, it can be seen that two very different

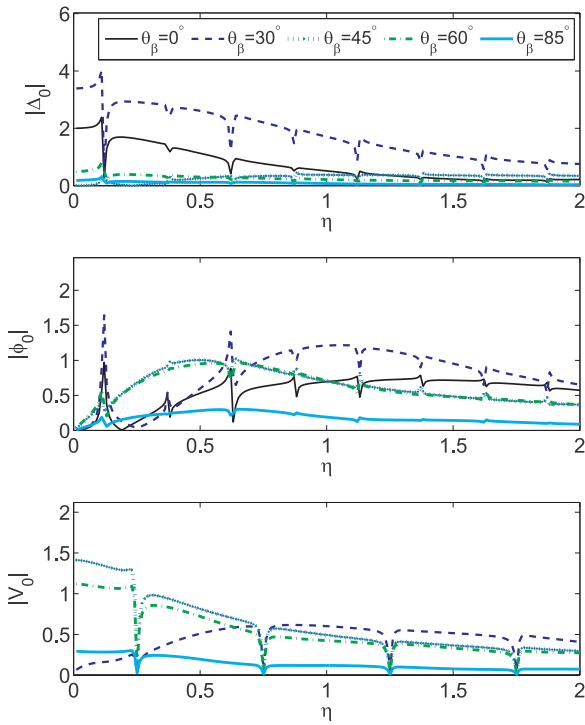


Fig. 6. Spectra of foundation displacements from "relaxed" solutions. $a/h = 1$, $W/H = 1$, $H/a = 2$, $m_b/m_f = 2$, and $\varepsilon = 4$.

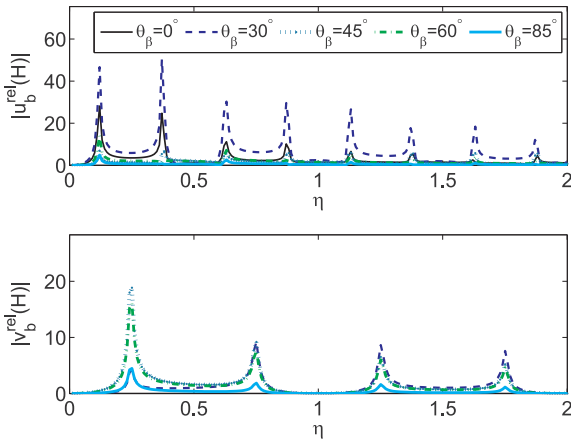


Fig. 7. Spectra of relative displacements of the shear wall from "relaxed" solutions. $a/h = 1$, $W/H = 1$, $H/a = 2$, $m_b/m_f = 2$, and $\varepsilon = 4$.

profiles that separate the case of $\theta_\beta < \theta_{cr}$ and $\theta_\beta > \theta_{cr}$ are exhibited, particularly in Figs. 2 and 6. For $\theta_\beta = 0^\circ$ and $\theta_\beta = 30^\circ$, in addition to the large response with high peak values near the first few natural frequencies (due to the coupling with the large horizontal translation of the foundation $|\Delta_0|$ at these two incident angles), $|\phi_0|$ do not grow as fast as in the cases of $\theta_\beta = 45^\circ$ and $\theta_\beta = 60^\circ$. In between the natural frequencies, the foundation rotations are significant when $\theta_\beta = 45^\circ$ and $\theta_\beta = 60^\circ$, with the local maxima at around $\eta \approx 0.5$ in Figs. 2 and 6. At $\theta_\beta = 85^\circ$, despite the smaller values at all frequencies, $|\phi_0|$ also has similar behavior as $\theta_\beta = 45^\circ$ and $\theta_\beta = 60^\circ$. The differences between these two types of behavior become less apparent for a taller shear wall as shown in Figs. 4 and 8, in which it can be seen that the local maxima of $|\phi_0|$ for $\theta_\beta = 45^\circ$ and $\theta_\beta = 60^\circ$ occur near $\eta \approx 1.1$.

In the range where η is smaller than the first horizontal/vertical resonant frequencies, $|\Delta_0|$ and $|u_b^{rel}(H)|$ are larger when the incident angle makes $|u_x^f(z=0)|$ larger; similarly, $|V_0|$ and $|v_b^{rel}(H)|$ are larger when the incident angle makes $|u_z^f(z=0)|$ larger. This order starts to change beyond the first resonant frequency due to the interplay

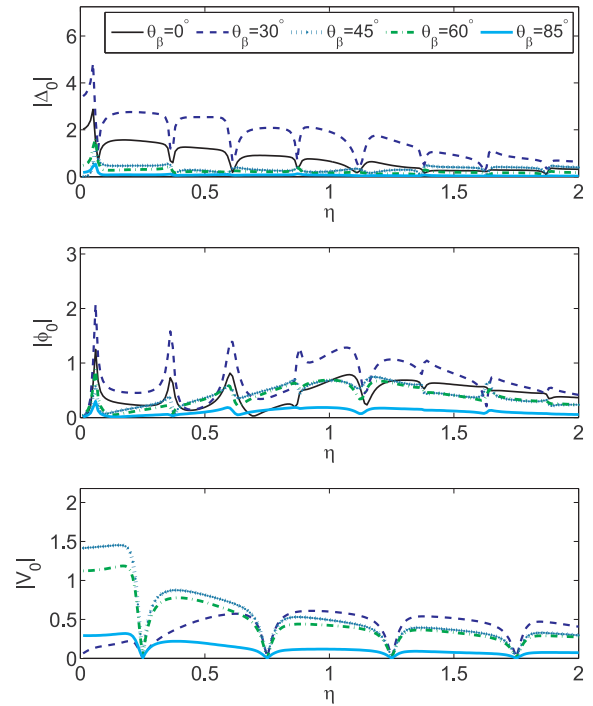


Fig. 8. Spectra of foundation displacements from "relaxed" solutions. $a/h = 1$, $W/H = 0.25$, $H/a = 8$, $m_b/m_f = 8$, and $\varepsilon = 4$.

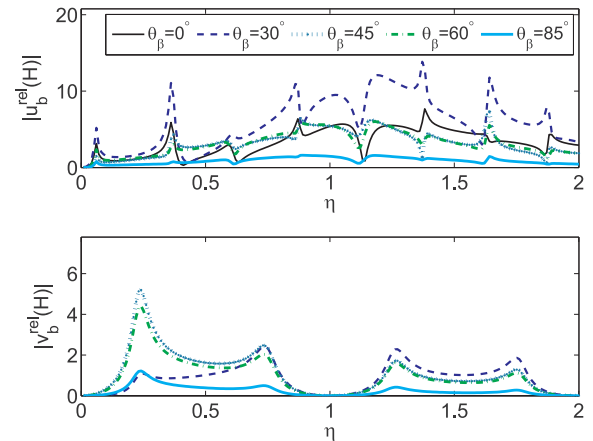


Fig. 9. Spectra of relative displacements of the shear wall from "relaxed" solutions. $a/h = 1$, $W/H = 0.25$, $H/a = 8$, $m_b/m_f = 8$, and $\varepsilon = 4$.

between the foundation filtering effect and the interactions previously described. The order change is especially prominent for $|V_0|$ when η is approaching 2 in Figs. 2, 4, 6 and 8.

Comparing the spectra of a taller shear wall with those of the square wall (comparing Figs. 8 and 9 with Figs. 6 and 7, or Figs. 4 and 5 with Figs. 2 and 3), it can be seen that for the taller shear wall, the first peaks of $|\Delta_0|$ and $|\phi_0|$ shift more toward lower frequencies with the slightly higher peak value for $|\Delta_0|$. The most dramatic changes for the taller shear wall are in the spectra of $|u_b^{rel}(H)|$: the first few peak values are considerably reduced from the corresponding square shear wall, with the first peak being more than 5 times smaller. In between natural frequencies in the range from $\eta \approx 0.8$ to $\eta \approx 1.4$, the value of $|u_b^{rel}(H)|$ can be larger than the first few peak values in the same spectrum. This region also corresponds to a relatively larger $|\phi_0|$ compared with other frequencies away from resonance.

Comparing the results with a shallow foundation to those of a semi-circular foundation (comparing Figs. 2 and 3 with Figs. 6 and 7 for the square shear wall, or Figs. 4 and 5 with Figs. 8 and 9 for the tall shear

wall), it can be seen that for a shallower foundation depth with $\theta_\beta = 0^\circ$ and $\theta_\beta = 30^\circ$, $|\Delta_0|$ decreases in a slower rate as η increases for the whole frequency range $0 < \eta \leq 2$. However, $|u_b^{rel}(H)|$ and $|v_b^{rel}(H)|$ are smaller at lower frequencies with the smaller peak values, and the first peak of $|v_b^{rel}(H)|$ at $\theta_\beta = 30^\circ$ even disappears as can be seen in Figs. 3 and 7. As for rotation, the change of $|\phi_0|$ highly depends on the incident angle: at $\theta_\beta = 45^\circ$ and $\theta_\beta = 60^\circ$, $|\phi_0|$ grows to a larger local maxima (the approximate location of the local maxima are unchanged: at around $\eta \approx 0.5$ for square shear wall; $\eta \approx 1.1$ for tall shear wall) as η increases from zero; but at $\theta_\beta = 30^\circ$, regardless of the larger response at the second resonance near $\eta = 0.375$, $|\phi_0|$ is smaller beyond $\eta \approx 0.8$ away from resonant frequencies.

5. Summary

This paper presents results based on an approximate analytic procedure for solving the 2-dimensional, soil-structure-interaction problem excited by an incident plane SV wave. The approximation is based on relaxing the zero-stress boundary conditions on the half-space surface. It is shown that under such conditions, the wave function expansion becomes simple, and only half of the series representation for the scattered waves is required. Also, the closed-form solution depends only on finite-dimensional matrices and is easy to compute.

For cases of semi-circular foundation and shallow foundation when the incidence is below critical, numerical results on foundation displacements and shear wall responses agree well with those of [3]. For cases of shallow foundation when incident angles are beyond critical, numerical results are presented here for the first time. The agreement between the cases presented in this paper and those in [3] suggest that the free-surface boundary conditions are indeed not as essential as other conditions that govern the solution (the continuity of displacements along the contact surface between the half-space and foundation, and

the dynamic equilibrium of the foundation). This result also supports the results of [7], which suggests that the solution to the model obtained from relaxed surface conditions may be similar to the solution in which a cylindrical approximation of the ground surface is made.

References

- [1] Enrique Luco J. Dynamic interaction of a shear wall with the soil. *J. Eng. Mech. Div.* 1969;95:333–46.
- [2] Trifunac MD. Interaction of a shear wall with the soil for incident plane SH waves. *Bull. Seismol. Soc. Am.* 1972;62(1):63–83.
- [3] Todorovska MI, Trifunac MD. Analytical Model for in Plane Building-Foundation-Soil Interaction: Incident P-, SV-, and Raleigh Waves, Report No. 90-01, Dept. of Civil Engrg, Univ. of Southern California, pp. 122 (1990).
- [4] Todorovska MI, Trifunac MD. In-plane foundation-soil interaction for embedded circular foundations. *Soil Dyn. Earthq. Eng.* 1993;12:283–97.
- [5] Todorovska Maria I, Trifunac MD. Effects of the wave passage and the embedment depth for in-plane building-soil interaction. *Soil Dyn. Earthq. Eng.* 1993;12:343–55.
- [6] Todorovska MI. Effects of the depth of the embedment on the system response during building-soil interaction. *Soil Dyn. Earthq. Eng.* 1992;11:111–23.
- [7] Todorovska Maria I, Rjoub Yousef AL. Plain strain soil-structure interaction model for a building supported by a circular foundation embedded in a poroelastic half-space. *Soil Dyn. Earthq. Eng.* 2006;26:694–707.
- [8] Lin Chi Hsin, Lee Vincent W, Todorovska Maria I, Trifunac Mihailo D. Zero-stress, cylindrical wave functions around a circular underground tunnel in a flat, elastic half-space: incident P waves. *Soil Dyn. Earthq. Eng.* 2010;30(10):879–94.
- [9] Zhang Chao, Liu Qijian, Deng Peng. Surface motion of a half-space with a semi-cylindrical canyon under P, SV, and Rayleigh waves. *Bull. Seismol. Am.* 2017;107(2):1–13.
- [10] Gičev Vlado, Trifunac Mihailo D, Orbović Nebojša. Translation, torsion, and wave excitation of a building during soil-structure interaction excited by an earthquake SH pulse. *Soil Dyn. Earthq. Eng.* 2015;77:391–401.
- [11] Gičev Vlado, Trifunac Mihailo D, Orbović Nebojša. Two-dimensional translation, rocking, and waves in a building during soil-structure interaction excited by earthquake P-wave pulse. *Soil Dyn. Earthq. Eng.* 2016;90:454–66.
- [12] Gičev Vlado, Trifunac Mihailo D, Orbović Nebojša. Two-dimensional translation, rocking, and waves in a building during soil-structure interaction excited by a plane earthquake SV-wave pulse. *Soil Dyn. Earthq. Eng.* 2016;88:76–91.